ELSEVIER

Nuclear Instruments and Methods in Physics Research B 195 (2002) 55–63

NIM B
Beam Interactions with Materials & Atoms

www.elsevier.com/locate/nimb

The unitary convolution approximation for heavy ions

P.L. Grande [a,*], G. Schiwietz [b]

[a] *Instituto de Física da Universidade Federal do Rio Grande do Sul, Avenida Bento Goncalves 9500, 91501-970 Porto Alegre, Brazil*
[b] *Bereich F, Hahn-Meitner-Institut Berlin, Glienicker Strasse 100, D-14109 Berlin, Germany*

Received 29 September 2001; received in revised form 20 November 2001

Abstract

The convolution approximation for the impact-parameter dependent energy loss is reviewed with emphasis on the determination of the stopping force for heavy projectiles. In this method, the energy loss in different impact-parameter regions is well determined and interpolated smoothly. The physical inputs of the model are the projectile-screening function (in the case of dressed ions), the electron density and oscillators strengths of the target atoms. Moreover, the convolution approximation, in the perturbative mode (called PCA), yields remarkable agreement with full semi-classical-approximation (SCA) results for bare as well as for screened ions at all impact parameters. In the unitary mode (called UCA), the method contains some higher-order effects (yielding in some cases rather good agreement with full coupled-channel calculations) and approaches the classical regime similar as the Bohr model for large perturbations ($Z/v \gg 1$). The results are then used to compare with experimental values of the non-equilibrium stopping force as a function of the projectile charge as well as with the equilibrium energy loss under non-aligned and channeling conditions.

PACS: 34.50.Bw; 61.85.+p; 34.50. Fa; 79.20.Rf
Keywords: Stopping power; Energy loss; Channeling

1. Introduction

The electronic energy loss has been studied for many years because of its direct application in problems concerning material damage, ion beam analysis and plasma physics. The theoretical treatment of the energy loss in atomic collisions has been greatly improved over the last decades. Calculations of the electronic energy loss have been performed by using traditional methods known from atomic physics investigations such as the plane wave Born approximation (PWBA) [1], the high-energy solution by Bethe [2] and the semi-classical approximation (SCA) [3]. More advanced models are the continuum distorted wave (CDW-EIS) [4], the classical trajectory Monte Carlo (CTMC) [5,6], the ACAM-CKLT model based on Liouville and Wigner equations in phase space [7] and finally the atomic orbital coupled-channel method (AO) [8–10] that yields reliable values for the impact-parameter dependent electronic energy loss. These methods based on atomic physics calculations offer reliable ways to obtain detailed

* Corresponding author.
E-mail addresses: grande@if.ufrgs.br (P.L. Grande), schiwietz@hmi.de (G. Schiwietz).
URL: www.hmi.de/people/schiwietz.

0168-583X/01/$ - see front matter
PII: S0168-583X(01)01164-8

information on the energy-loss processes in gases as well as for the inner-shell electrons of solids. Of course, other approaches have to be adopted for conduction-band electrons of solid-state targets [11–14] in order to obtain an accurate description of the energy loss due to the valence electrons. Other models such as those of [15–18] have strongly enlarged our understanding on the physical energy loss processes.

During the last years we have investigated the electronic energy loss of bare and screened ions for light targets using the coupled-channel method. This first principle calculation [8–10], based on an expansion of the time dependent electronic wave function in terms of atomic orbitals, has been successfully applied to evaluate the impact-parameter and angular dependence of the electronic energy loss and the total stopping cross-section of ions (anti-protons, H and He) colliding with H and He atoms at energies of 1–500 keV/amu. It has also been applied to calculate the entrance-angle dependence of the stopping force for He ions channeling along the Si main crystal directions [19].

These benchmark calculations are being used to check simplified models that account for the basic energy loss processes without the need of large scale calculations [20,21]. In particular, simple models for the impact parameter dependent energy loss are needed to be included in computer simulation codes as well as for channeling data analysis.

In the present work, we give a review on the unitary convolution approximation (UCA) applied to stopping of heavy ions. This simple model yields accurate results for the electronic energy loss from small to large impact parameters. The physical inputs are the electron density and oscillators strengths of the atoms. In the following, we describe in detail the UCA model, in particular the treatment of projectile screening and charge-states, which are very important for heavy projectiles carrying many electrons. In Section 3, we discuss our numerical results for the equilibrium mean stopping cross section and recent pre-equilibrium stopping data for carbon foils [22,23]. If not indicated otherwise, atomic units (1 a.u. $= e = m = \hbar$) will be used throughout the paper.

2. Unitary convolution approximation

The convolution approximation method (UCA) [24] is reviewed with full details concerning the projectile screening and charge-states, which are essential ingredients for stopping of heavy projectiles.

In recent works [20,21], we have proposed a simple formula for the impact parameter dependent energy loss $Q(b)$,

$$Q(b) = \int \mathrm{d}^2 r_\perp K(\vec{b} - \vec{r}_\perp) \int \mathrm{d}z\, \rho(\vec{r}_\perp, z), \tag{1}$$

which describes a convolution of the electronic density $\rho(\vec{r})$ integrated along the ion path z, with a kernel K given by

$$K(b_\mathrm{e}) = \frac{2Z^2}{v^2 b_\mathrm{e}^2} h(2v b_\mathrm{e}/\eta) \sum_i f_i g\left(\frac{\omega_i b_\mathrm{e}}{v}\right). \tag{2}$$

This kernel determines the energy gain of a point-like electron at a distance b_e from the projectile path. It joins smoothly all regions of impact parameters b for which two-body ion–electron (small b) and dipole (large b) approximations can be used. The function $h(x)$ (see Appendix A) approaches zero for $x \ll 1$ and reaches 1 for large values of x.

The first two terms in Eq. (2) stem from violent binary electron–projectile collisions, namely the scattering of a quasi-free target electron by the projectile potential. For $\eta = 1$ they corresponds to the energy transfer in first-order perturbation theory and vanish for relative impact parameter b_e smaller than the electron de Broglie wavelength in the projectile frame. In addition, with an appropriate choice of η these terms resemble the classical energy transfer to a statistical distribution of electrons at rest. The last term, involving the g function (see Appendix A), the transition energies ω_i and the corresponding oscillator strengths f_i, accounts for the long ranged dipole transitions.

The first integral $\int \mathrm{d}^2 r_\perp, \ldots,$ in Eq. (1) describes a convolution with the initial electron density also outside the projectile path and yields non-local contributions to the energy loss. With the parameter η equal to one, this formula reproduces virtually full first-order Born (SCA) calculations for bare [20] and well as for screened projectiles [25]

and is denoted PCA (perturbative convolution approximation). For increasing projectile charges there is a break-down of all first order theories (on which PCA is based). They do not take in account, for instance, that each electronic transition gives rise to an increased final-state population and a corresponding reduction of the initial state population. It is clear that the ionization probability cannot increase indefinitely with the strength of the perturbation (the so-called saturation effect). Since these excess ionization processes are related to small impact parameters, we use a scaling parameter η in the function h to reproduce the total stopping cross-section for bare ions as given by the Bloch model [16]. Since the Bloch model originates from a non-perturbative solution of the Schrödinger equation in the projectile frame, the present model will also conserve unitarity. Thus, the scaling factor η is obtained from

$$\eta = \exp\left[\mathrm{Re}\,\psi(1+\mathrm{i}\kappa) - \psi(1)\right] \tag{3}$$

$$= \exp\left[\kappa^2 \sum_{l=1}^{\infty} \frac{1}{l(l^2+\kappa^2)}\right], \tag{4}$$

with $\kappa = Z_{\mathrm{eff}}/v$ (Z_{eff} is equal to the projectile nuclear charge Z for bare ions). The projectile screening is taken into account for distant collisions (through the g function, see Appendix A) as well as for close collisions by using an impact-parameter dependent effective charge Z_{eff} [26], according to

$$Z_{\mathrm{eff}}(b) = Z - n_{\mathrm{e}}\Phi(b), \tag{5}$$

where $\Phi(r)$ is the projectile-screening function, and n_{e} is the number of projectile bound electrons. With the scaling factor η (from Eq. (3)), the stopping force turns out to be identical to the Bloch stopping formula [16] for bare ions at high projectile speed. Further, $K(b_{\mathrm{e}})$ in Eq. (2) resembles the impact parameter dependent Bohr energy loss formula for $\kappa \gg 1$. In this way, for bare ions the present energy-loss model Eqs. (1)–(4) is the impact-parameter realization of the Bethe–Bloch formula.

Fig. 1 shows the product ansatz from Eq. (2) that interpolates smoothly between small and large impact-parameter solutions, represented by dotted and dashed lines respectively for collisions of

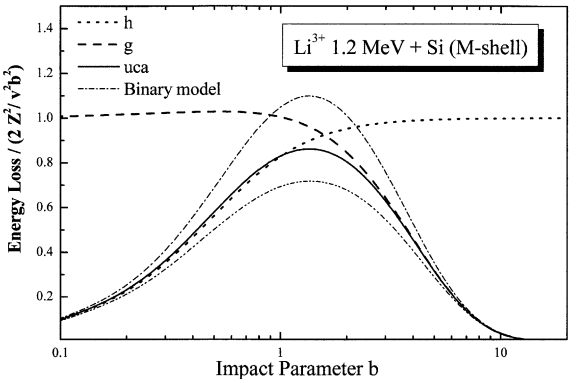

Fig. 1. Interpolation between close collisions, h function ($\cdots$), and distant collisions, g function (- - -). Solid line: present UCA method according to the product ansatz in Eq. (2). Dash-double-dotted lines: binary model for bare Li ions and anti-Li [18] (see text).

1.2 MeV Li^{3+} ions on Si M-shell electrons. For comparison a rather different interpolation schema is used in the binary model [18] that contains polarization effects (Barkas term) for Li, dash-dot-dotted line, and anti-Li, dash-double-dotted line. It is pointed out, that the present UCA interpolation does not contain any polarization effects [27]. As a consequence, energy-loss results for particles and anti-particles are the same. Indeed, this fact has allowed for a clear separation of the Barkas effect for He and Li ions under channeling conditions [27]. Nevertheless, for heavier projectiles the Barkas effect strongly saturates and should be of minor importance [28].

2.1. Projectile screening

In the present model for heavy projectiles, the screened projectile potential V_{p} has been determined by the expression

$$V_{\mathrm{p}}(\vec{r}) = -\frac{Z}{r} + \sum_{j}^{n_{\mathrm{e}}} \int \mathrm{d}^3 r' \frac{|\phi_j(\vec{r}')|^2}{|\vec{r}-\vec{r}'|}, \tag{6}$$

where ϕ_j are the projectile–electron wave functions. In principle, exchange and correlation potentials have to be added, but these contributions vanish in the high-velocity limit. The numerical wave functions ϕ_j for each electron j of the projectile are obtained according to the Hartree–Fock–Slater (HFS) procedure [29]. The potential

has been fitted using a general expression consisting of sum of generalized single-zeta potentials according to

$$V_{\mathrm{p}}(\vec{r}) = -\left(\frac{Z-n_{\mathrm{e}}}{r} + \frac{n_{\mathrm{e}}}{r}\Phi(r)\right), \tag{7}$$

with

$$\Phi(r) = \sum_{n=1}^{n_{\max}} (A_n + B_n r)\exp(-C_n r), \tag{8}$$

where the coefficients A_n, B_n and C_n are fitting parameters. The number of generalized single-zeta potentials, $n_{\max}$, usually corresponds to the number of electronic sub-shells of projectile.

A much simpler method, that gives very similar results for the projectile screening function, is just to consider the scaled projectile function

$$\Phi(r) = \Phi_{\mathrm{neutral}}(r/a) \tag{9}$$

with an approximate screening length $a = 1 - q/Z$ or $(a = n_{\mathrm{e}}/Z)$ (taken from [30]), where q is the projectile charge-state and Φ_{neutral} is the screening function for the corresponding neutral projectile. It has been tabulated for all elements, for instance using Dirac–Hartree–Fock–Slater (DHFS) calculations, in [31], as a sum of exponentials functions.

It is important to point out that the projectile electrons screen the projectile nucleus as spectators of the target excitation, i.e. the projectile electrons remain in the ground-state when the target is excited. Thus, we also neglect the so-called anti-screening effect, where the electron–electron interaction between the bound projectile electrons and the target electrons results in an enhancement of the ionization and excitation cross sections at intermediate to high energies [32]. For the case of charge-state equilibrium the bound projectile electrons are at least as fast as the projectile according to the stripping Bohr criterion. On the other hand, there is a kinematical suppression of the anti-screening for projectiles slower than the mean orbital velocity. In this way, the anti-screening effect is generally of minor importance for energy loss calculations (see also [30]).

The UCA model in the perturbative mode ($\eta = 1$) reproduces the results of first-order Born SCA [20]. Only for very small impact parameters ($b \ll r_{\mathrm{shell}}$, r_{shell} is the shell radius), some deviations may be found, being more significant for projectile velocities at or below the mean orbital velocity for a given shell [25]. The reason is the influence of the initial momentum distribution of the target electrons (shell corrections), which is not fully included in the present model and leads to an overestimated innershell contribution to the calculations. This reflects the limitation of the UCA model that is strictly valid for projectile speeds exceeding the mean electron orbital velocity by far. Concerning higher-order effects, comparisons with coupled-channel calculations show that the UCA model provides reliable energy loss values for small as well as for large perturbations, as shown in [21,26]. Nevertheless, higher-order effects related to polarization (Barkas effect) or to the Fermi–Shuttle effects (electron-energy diffusion due to multiple interactions [6]) are not accounted in the present model.

3. Comparison with measurements

In order to provide a comparison with experimental data the impact-parameter-dependent energy loss $Q(b)$ from Eq. (1) has to be integrated over all impact parameters according to the ion flux distribution. In the case of random materials or non-aligned directions in crystals, the ion flux distribution is uniform, but along a crystal axis or plane it has to be calculated by solving Newton's equations for an ensemble of ions. Furthermore, depending on the experimental conditions, the energy loss can be determined in an pre-equilibrium stage, for a frozen projectile charge state and without any charge-changing process [22,23,33,34].

However, most of the energy loss data have been determined for charge-state equilibrium. This means that the measured energy loss corresponds to an average value over all projectile charge-states according to the charge-state fractions f_q. In addition, for this case, the energy loss due to projectile electron-loss processes has to be also included. In general, the mean equilibrium stopping force is given by

$$\left(\frac{dE}{dx}\right)_{\text{equilibrium}} = \sum_q f_q \left(\left(\frac{dE}{dx}\right)_{\text{target}}(q) + \left(\frac{dE}{dx}\right)_{\text{projectile}}(q) \right), \tag{10}$$

where the first term above in the sum corresponds to the stopping force for target ionization/excitation and capture due to a projectile with a well defined initial charge-state q (note that we have excluded capture processes in this work). The second term $(dE/dx)_{\text{projectile}}$ represents the stopping force due projectile ionization and excitation. In some energy-loss approaches, this last term is not taken into account and the stopping force evaluated for the mean-charge state replaces the sum over the charge-state distribution. As we will observe, this may lead to wrong energy loss predictions.

It should be stressed that the fractions f_q represent the projectile charge-states that have been measured far behind foil targets. These fractions are affected by projectile inner-shell vacancies and multiply excited states that lead to Auger-transitions outside the target. On the other hand, excited projectiles inside the solid will be less screened. In this work, this effect is partially accounted for by taking the external charge-state distributions (after all Auger decays). In what follows we will compare the UCA calculations with experimental equilibrium and non-equilibrium (frozen charge-state) stopping data.

3.1. Equilibrium stopping

Fig. 2 shows experimental data of different groups [35] for the equilibrium total stopping force of oxygen in Al, in comparison with UCA calculations discussed above. The solid line corresponds to calculations according to Eq. (10), with the charge-state fractions estimated from [36] by considering a gauss distribution around the mean charge-state q_{mean} with standard deviation obtained from a fitting formula given in [36]. The oscillator strengths for Al were calculated using the procedure stated in [20] to deliver the ICRU I

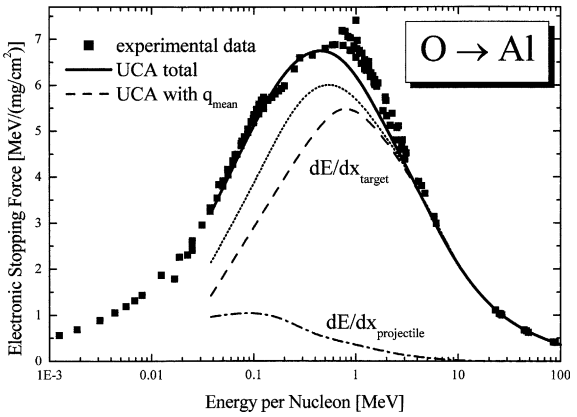

Fig. 2. Mean equilibrium stopping force for oxygen in aluminium. Experimental data compilation from [35]. Lines indicate the present UCA calculations for the total stopping according to Eq. (10) (—), stopping due to target electrons only using the charge-state fractions (· · ·), the mean-charge-state approximation (- - -) and the stopping due to projectile ionization/excitation (– · – · –·).

value. In the case of projectile excitation/ionization, the stopping force values have been calculated by exchanging the role of projectile and target and by using the HFS procedure to determine electron density, binding energies and oscillator strengths for all projectile charge-states. For the present case the correct use of three-body collision kinematics for the projectile ionization leads to small corrections only (less than 1% for the total stopping force). Except for intermediate incident energies, there is a very good agreement between experimental and theoretical data. At energies around 1 MeV/u the model predictions underestimate the experimental data by up to 10%.

Most likely, the deviations between experimental and theoretical results corresponds to a sum of all effects that are not considered in the present UCA calculations such as polarization (Barkas effect), the Compton profile of the inner-shell electrons (shell corrections), or electron capture into bound projectile states. For much lower energies, around 0.1 MeV/u, the agreement might be accidental due to a compensation of some of the effects cited above. An inspection of this figure also shows how important is the role of the charge-state distribution on the determination of the total stopping force. A model (dashed line) that uses

just a fixed mean charge state of the projectile for $(dE/dx)_{target}$, (without averaging over the charge-state distribution) and $(dE/dx)_{projectile} = 0$ (in Eq. (10)) predicts reliable stopping values only for energies higher than 2 MeV/u, and for lower energies very strong deviations are observed. Uncertainties of about 20% (between dashed and dotted lines) result from the replacement of the charge-state distribution by a mean charge state for the target ionization/excitation. Finally it is also observed that the energy loss contribution due to projectile ionization/excitation reaches about 30% at energies around 0.04 MeV/u.

Similar results are shown in Fig. 3 for the random stopping force in equilibrium for oxygen ions in silicon. The overall agreement is even better for energies higher than 3000 keV (about 0.2 MeV/u). For this case, we have taken the experimental charge-state fractions from [38]. But also in this case the good agreement is expected to be accidental due to a partial compensation of polarization effects and capture processes, which would increase the stopping and shell corrections, which would decrease the stopping.

In order to better clarify this issue we compare the stopping under channeling conditions, namely

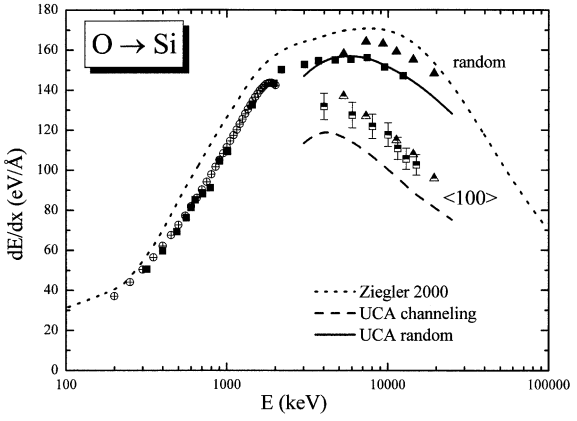

Fig. 3. Mean equilibrium stopping force for oxygen in silicon under non-aligned and under channeling conditions. Experimental data taken from [28,37–39] (symbols). Lines represent the values for the total stopping according to the SRIM code [40] (···) and the UCA method for random (—) and channeling ⟨100⟩ direction (- - -).

for O ions channeling along Si ⟨1 0 0⟩ directions. In contrast to the random stopping case, the UCA calculations do not agree with the experimental channeling data (the deviations are much larger for channeling Li ions [27]). This comes from the fact that under channeling conditions, all energy-transfer processes arising from the Si inner electrons are strongly suppressed. Thus, capture and shell corrections play only a minor role and the difference between the experimental channeling data and the UCA calculations is attributed to the Barkas effect only [27].

For oxygen channeling along the Si ⟨1 0 0⟩ direction the Barkas effect amounts to 10% [28] of the total stopping whereas for Li ions, also in Si, much larger relative values have been found. For light ions (up to Li) around 0.5 MeV/u perturbative treatments of the polarization effect work quite well, but for O ions only non-perturbative methods can be used to explain the strong saturation observed [28].

It should be stressed that similar agreement for the random stopping force is also obtained by the recently developed binary model [18]. In fact, this model includes shell corrections and contains polarization effects, and thus, it can be used for much lower energies compared to the UCA model. However, a proper representation of the spatial distribution of the target electrons in their undisturbed state is missing in the binary theory. On the other hand, the main feature of the UCA model is its impact-parameter dependence prediction, and as a consequence, its improved description of the stopping under channeling conditions. In fact, both theories are incomplete but complementary when it comes to application in channeling.

3.2. Pre-equilibrium stopping

Experimental data for the energy loss without charge-changing processes have been recently determined and provide the best check for theoretical models. In Fig. 4 the experimental stopping data [22] are displayed as a function of the square of the projectile-charge for 2 MeV/u Ne ions in carbon foils. Special experimental procedures have been used to isolate the energy loss for a pure charge-state q [22]. The UCA calculations are in good

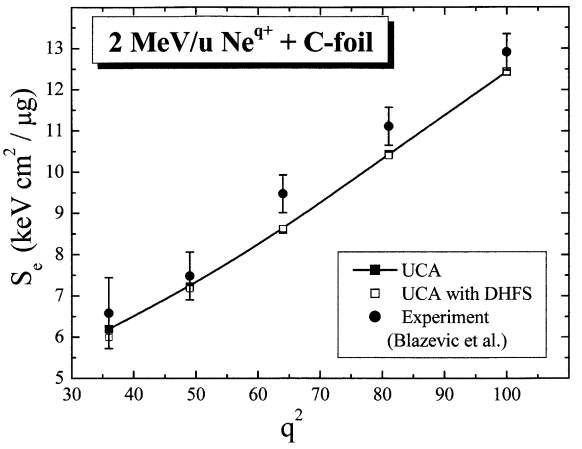

Fig. 4. Pre-equilibrium stopping for pure charge-states q of 2 MeV/u Ne in carbon. Two projectile screening functions have been used in the UCA calculations: HFS screening functions for each charge-state (■) and scaled neutral DHFS potentials as defined by Eq. (9) and [31] (□).

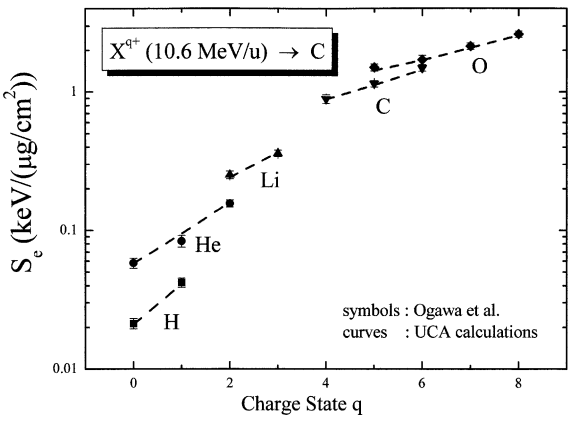

Fig. 5. Pre-equilibrium stopping for H^0, H^+, He^0, He^+, He^{2+}, Li^{2+}, Li^{3+}, C^{4+}, C^{5+}, C^{6+}, O^{5+}, O^{6+}, O^{7+}, O^{8+} at 10.6 MeV/u on carbon. The symbols correspond to measurements of Ogawa et al. [23] and the dashed curves to UCA calculations.

agreement with experimental data. On the average, the theoretical results are slightly below the data points, which is attributed to a small influence of the Barkas effect. Here we also show by open squares the UCA calculations using the scaled projectile screening from Eq. (9). As can be observed, the use of both projectile screening functions (from Eqs. (6) and (7) provides nearly the same energy loss results.

Fig. 5 presents the experimental data of Ogawa et al. [23] for the pre-equilibrium stopping force at high projectile energies (10.6 MeV/u) in comparison with UCA calculations for H, He, Li, C and O with different charge states. As in Fig. 4 full oscillator strengths for each C sub-shell have been taken into account. Again, rather good agreement between the experimental data and the UCA calculations is observed. These measurements provide the best scenario of applicability of the UCA method, which is, high projectile speeds (in comparison with the mean electron one) and frozen charge-states. Furthermore, at this projectile energy, the Barkas effect is of minor importance [28]. An inspection of this figure also shows a general trend that simplifies the treatment for much heavier projectiles. The higher the projectile charge-state q, the smaller is the difference among the stopping forces for distinct projectile nuclear charges. Thus, the stopping for highly charged projectiles will depend on q only, if the projectile screening radius is small compared to all target shell radii.

4. Conclusions

We have described calculations of the electronic energy loss using the UCA model. This non-perturbative method provides full information of the impact-parameter dependent energy loss of bare and screened particles for each target-subshell. Furthermore, it relies on simple formulas, allowing for a computer realization many orders of magnitude faster than the full numerical solution of the time-dependent Schrödinger equation. Thus, it allows for energy loss calculations for each target-subshell and each projectile charge-state separately.

Experimental data for pre-equilibrium and equilibrium stopping are in very good overall agreement with the UCA model, even at low energies where the present model is not applicable. In such cases the good agreement is ascribed to be accidental due to cancellation of effects that are not included in the calculations, such as capture, polarization and shell corrections.

Acknowledgements

This work was partially supported by CAPES-PROBRAL 121/00 (Coordenação de Aperfeiçoamento de Pessoal de Nível Superior) and by the Alexander-von-Humboldt foundation.

Appendix A

The functions $h(x)$ and $g(x)$ correspond to analytical solutions for the energy transfer at small and large impact parameters and read

$$h(x) = \frac{x^2}{2}\int_0^1 \mathrm{d}y\, y K_0(xy^2) J_0(xy\sqrt{1-y^2}). \qquad (A.1)$$

and

$$g(x) = f_\parallel^2(x) + f_\perp^2(x), \qquad (A.2)$$

with

$$f_\parallel(x) = n_e/Z \sum_i \left(A_i K_1(x\delta_i) x\delta_i + x^2\beta_i\gamma_i K_0(x\delta_i)\right) + (1 - n_e/Z) x K_1(x), \qquad (A.3)$$

$$f_\perp(x) = n_e/Z \sum_i \left(A_i x K_0(x\delta_i) + x^3\beta_i\gamma_i K_1(x\delta_i)/x\delta_i\right) + (1 - n_e/Z) x K_0(x). \qquad (A.4)$$

In the above equations, K_0 and K_1 are the modified Bessel functions, $\beta_i = B_i v/\omega$, $\gamma_i = C_i v/\omega$,$\delta_i = (1 + \gamma_i^2)^{1/2}$ (A_i, B_i and C_i are the fitting constants from Eq. (8)), ω is the transition energy. A similar expression for the distant collision function g was derived previously in [30] for the case $B_i = 0$ (Bohr or Yukawa potential).

References

[1] H.A. Bethe, R.W. Jackiw, Intermediate Quantum Mechanics, second ed., W.A. Benjamin, New York, 1968.
[2] H. Bethe, Ann. Phys. 5 (1930) 325.
[3] N.M. Kabachnik, V.N. Kondratev, O.V. Chumanova, Phys. Stat. Sol. (b) 145 (1988) 103.
[4] P.D. Fainstein, V.H. Ponce, A.E. Martinez, Phys. Rev. A 47 (1993) 3055.
[5] R.E. Olson, Rad. Eff. Deff. Solids 110 (1989) 1.
[6] P.L. Grande, G. Schiwietz, J. Phys. B: At. Mol. Opt. Phys. 28 (1995) 425.
[7] G. Maynard, K. Katsonis, C. Deutsch, et al., Nucl. Instr. and Meth. A 464 (2001) 86;
G. Maynard, G. Zwicknagel, C. Deutsch, et al., Phys. Rev. A 6305 (2001) 2903.
[8] G. Schiwietz, Phys. Rev. A 42 (1990) 296.
[9] P.L. Grande, G. Schiwietz, Phys. Rev. A 44 (1991) 2984.
[10] G. Schiwietz, P.L. Grande, Nucl. Instr. and Meth. B 69 (1992) 10;
P.L. Grande, G. Schiwietz, Phys. Rev. A 47 (1993) 1119.
[11] A.F. Lifschitz, N.R. Arista, Phys. Rev. A 57 (1998) 200;
J.E. Valdes, P. Vargas, N.R. Arista, Phys. Rev. A 56 (1997) 4781.
[12] I. Campillo, J.M. Pitarke, A.G. Eguiluz, Phys. Rev. B 58 (1998) 10307.
[13] J.J. Dorado, F. Flores, Phys. Rev. A 47 (1993) 3092.
[14] P.M. Echenique, R.M. Nieminem, R.H. Ritchie, Solid State Commun. 37 (1981) 779;
P.M. Echenique, R.M. Nieminem, J.C. Ashley, R.H. Ritchie, Phys. Rev. A 33 (1986) 897.
[15] N. Bohr, Philos. Mag. 25 (1913) 10;
N. Bohr, Phys. Rev. 59 (1941) 270.
[16] F. Bloch, Ann. Physik 16 (1933) 285.
[17] P. Sigmund, U. Haagerup, Phys. Rev. A 34 (1986) 892;
H.H. Mikkelsen, P. Sigmund, Phys. Rev. A 40 (1989) 101;
H.H. Mikkelsen, Nucl. Instr. and Meth. B 58 (1991) 136.
[18] P. Sigmund, A. Schinner, Eur. Phys. J. D 12 (2000) 425;
P. Sigmund, A. Schinner, Phys. Scripta T 92 (2001) 222;
P. Sigmund, A. Schinner, Fundam. Appl. Asp. Mod. Phys., in press.
[19] J.H.R. dos Santos, P.L. Grande, M. Behar, H. Boudinov, G. Schiwietz, Phys. Rev. B 55 (1997) 4332.
[20] P.L. Grande, G. Schiwietz, Phys. Rev. A 58 (1998) 3796.
[21] G. Schiwietz, P.L. Grande, Nucl. Instr. and Meth. B 153 (1999) 1.
[22] A. Blazevic et al., Nucl. Instr. and Meth. B, Submitted for publication;
A. Blazevic et al., Phys. Rev. A 61 (2000) 032901/1–6.
[23] H. Ogawa et al., Phys. Lett. A 167 (1992) 487;
H. Ogawa et al., Nucl. Instr. and Meth. B 82 (1993) 80;
H. Ogawa et al., Nucl. Instr. and Meth. B 115 (1996) 66;
H. Ogawa et al., Phys. Rev. A 54 (1996) 5027;
H. Ogawa et al., Nucl. Instr. and Meth. B 132 (1997) 36;
H. Ogawa et al., Phys. Rev. B 43 (1991) 11370.
[24] The computational implementation of the UCA method [20,21], CasP (convolution approximation for swift particles) program, is available at http://www.hmi.de/people/schiwietz/casp.html.
[25] G. de M. Azevedo, P.L. Grande, G. Schiwietz, Nucl. Instr. and Meth. B 164 (2000) 203.
[26] G. de M. Azevedo, M. Behar, J.F. Dias. P.L. Grande, D.L. da Silva, G. Schiwietz, Phys. Rev. B, in press.
[27] G. de M. Azevedo, P.L. Grande, M. Behar, J.F. Dias, G. Schiwietz, Phys. Rev. Lett. 86 (2001) 1482.
[28] L.L Araujo, P.L. Grande, M. Behar, J.F. Dias, J.H.R. dos Santos, G. Schiwietz, Submitted for publication.
[29] F. Herman, S. Skillmann, Atomic Structure Calculations, Prentice-Hall, Englewood Cliffs, NJ, 1963.

[30] P. Sigmund, Phys. Rev. A 56 (1997) 3781.
[31] F. Salvat, J.D. Martinez, R. Mayol, J. Parellada, Phys. Rev. A 36 (1987) 467.
[32] E.C. Montenegro, W.E. Meyerhof, J.H. McGuire, Adv. At. Mol. Opt. Phys. 34 (1994) 249.
[33] G. Dollinger, ICACS, Submitted for publication.
[34] N.E.B. Cowern et al., Nucl. Instr. and Meth. B 2 (1984) 112; N.E.B. Cowern et al., Nucl. Instr. and Meth. B 12 (1985) 43.
[35] H. Paul, http://www.exphys.uni-linz.ac.at/stopping.
[36] G. Schiwietz, P.L. Grande, Nucl. Instr. and Meth. B 175–177 (2001) 125.
[37] D.C. Santry, R.D. Werner, Nucl. Instr. and Meth. B 5 (1984) 449.
[38] W. Jiang, R. Grötzschel, W. Pilz, B. Schmidt, W. Möller, Phys. Rev. B 59 (1999) 226;
W. Jiang, R. Grötzschel, W. Pilz, B. Schmidt, W. Möller, Phys. Rev. B 60 (1999) 714.
[39] L.L Araujo, M. Behar, J.F. Dias, P.L. Grande, IBA, Submitted for publication.
[40] J.F. Ziegler, J.P. Biersack, U. Littmark, The Stopping and Range of Ions in Solids, Pergamon, New York, 1985, http://www.srim.org.